

Coupled optoelectronic simulation of organic bulk-heterojunction solar cells: Parameter extraction and sensitivity analysis

R. Häusermann,^{1,a)} E. Knapp,¹ M. Moos,¹ N. A. Reinke,¹ T. Flatz,² and B. Ruhstaller^{1,2,b)}

¹*Institute of Computational Physics, Zurich University of Applied Sciences, Wildbachstrasse 21, 8401 Winterthur, Switzerland*

²*Fluxim AG, Dorfstrasse 7, 8835 Feusisberg, Switzerland*

(Received 20 July 2009; accepted 24 September 2009; published online 18 November 2009)

A comprehensive optoelectronic device model for organic bulk-heterojunction solar cells is presented. First the optical incoupling into a multilayer stack is calculated. From the photon absorption profile a charge transfer exciton profile is derived. In this study we consider the Onsager–Braun mechanism to calculate the dissociation of the CT excitons into free charge carriers. These free charge carriers then migrate toward the electrodes under the influence of drift and diffusion. A general problem arising in computer simulations is the number of material and device parameters, which have to be determined by dedicated experiments and simulation-based parameter extraction. In this study we analyze measurements of the short-circuit current dependence on the active layer thickness and current-voltage curves in poly(3-hexylthiophene):[6,6]-phenyl-C₆₁-butyric acid methyl ester based solar cells. We have identified a set of parameter values including dissociation parameters that describe the experimental data. The overall agreement of our model with experiment is good, however, a discrepancy in the thickness dependence of the current-voltage curve questions the influence of the electric field in the dissociation process. In addition transient simulations are analyzed which show that a measurement of the turn-off photocurrent can be useful for estimating charge carrier mobilities. © 2009 American Institute of Physics. [doi:10.1063/1.3259367]

I. INTRODUCTION

After the huge progress organic light-emitting diodes have made in the last years, organic photovoltaic (OPV) devices attract more and more interest. State of the art OPV devices yield an energy conversion efficiency of around 6%–7% for single junction cells¹ as well as tandem cells.² This is much less compared to other already established photovoltaic power conversion techniques which have an efficiency above 10% or even above 20% for crystalline silicon cells. Nevertheless OPV devices have several advantages such as the possibility of low-cost production,³ room temperature processing, and thin film structures. The latter two make it possible to use flexible substrates and thus the production of flexible solar cells. This leads to low-cost, flexible, and transportable energy generators. Our research focuses on the influence of optical and electrical parameters on device performance.

The field of OPVs can be separated into the planar-heterojunction devices where the donor and acceptor materials are deposited one after the other, mostly by evaporation of small molecules and the bulk-heterojunction (BHJ) devices, where the two organic materials are diluted in the same solvent and spin coated as one layer. The advantage of the BHJ structure is that most of the generated excitons reach a nearby donor-acceptor interface where they dissociate into free charge carriers. This efficient exciton harvesting leads to higher power conversion efficiencies for BHJ devices.

Numerical models for organic BHJ devices provide insight into operating mechanisms and allow for device structure optimization. The simulation of OPV devices can be separated into two parts, firstly there is the incoupling of light into a multilayer structure and secondly the extraction of charges which needs an electrical model. The absorption of light within the multilayer structure is a crucial process and thus one of the main areas of numerical simulations. Harrison *et al.*⁴ used analytical models and compared them to measured photocurrent action spectra. Later a transfer matrix formalism has been used by Petterson *et al.*⁵ to calculate the absorbed optical energy within the multilayer structure. This formalism is widely used to optimize layer structures for single junction⁶ as well as tandem cells.⁷ Although optical models are very reliable they are only able to give an upper limit of the achievable photocurrent. Therefore, electrical models have been developed to study charge generation and transport losses in planar heterojunction⁸ as well as BHJ devices.^{9–12} These models differ in their choice of ingredients, definition of the boundary conditions, as well as in their methods to solve the drift-diffusion equations. Coupled optoelectronic models have been introduced by Kirchartz *et al.*,¹³ Lacic *et al.*,¹⁴ and Kotlarski *et al.*,¹⁵ where they connected a drift-diffusion solver with an optical thin film simulator. All the electrical models mentioned are one dimensional models and they treat every layer as an effective medium, i.e., a homogenous layer.

In this study we present a comprehensive numerical model which considers optical as well as electrical effects. This device model has originally been developed for the analysis of organic-light-emitting diodes^{16–18} and was com-

^{a)}Electronic mail: hroger@phys.ethz.ch. Present address: Laboratory for Solid State Physics, ETH Zurich, 8093 Zurich, Switzerland.

^{b)}Electronic mail: beat.ruhstaller@zhaw.ch.

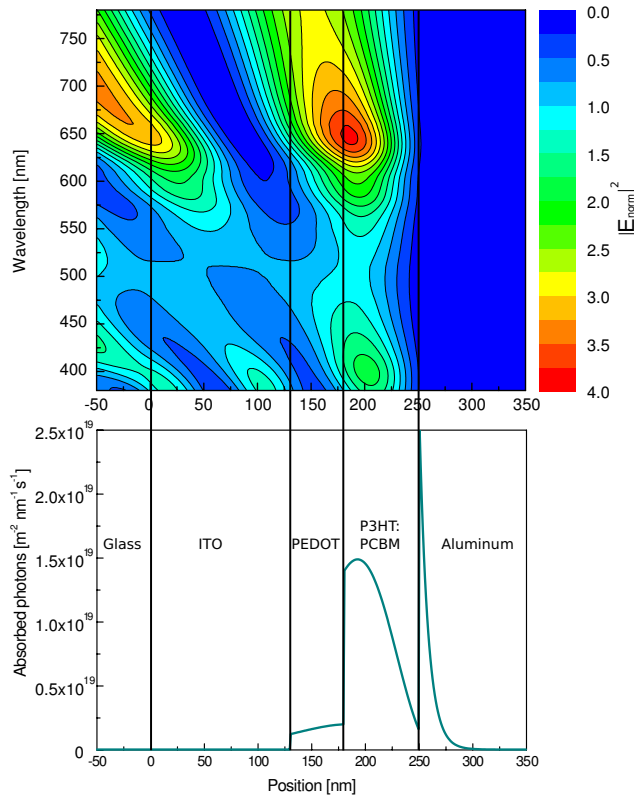


FIG. 1. (Color online) Electromagnetic field penetration plot (top) is calculated using a transfer matrix formalism. This field penetration is then used to derive the photon absorption rate profile (bottom).

mercialized afterward. This software, SETFOS,¹⁹ has been extended for the simulation of organic BHJ solar cells.

II. DESCRIPTION OF THE NUMERICAL DEVICE MODEL

A. Optical modeling

OPV cells consist of a multilayer structure, with layer thicknesses on the order of the wavelength of the incident light, which is shorter than the coherence length of sunlight. Therefore an OPV is an optically coherent device. This gives rise to interference effects inside the device which can be exploited to increase the maximum photocurrent by carefully tuning the thicknesses of the individual layers.^{20,5,10} An approach to find the optimal layer thicknesses from an optical point of view is to calculate the electromagnetic field inside the multilayer stack using a transfer matrix formalism. This approach has been used in the optical simulation of OLEDs^{16,18} and OPVs (Ref. 5) and is well established in the field of organic electronics. With this formalism the normalized optical electric field E_{norm} is calculated throughout the multilayer stack (cf. Fig. 1). For plane waves, the optical field intensity within the stack is given by

$$I = \frac{1}{2} \epsilon_0 c n |E|^2. \quad (1)$$

In the transfer matrix formalism we normalize the incident electric field such that the incoming electric field amplitude is 1. Therefore, the electric field calculation gives the

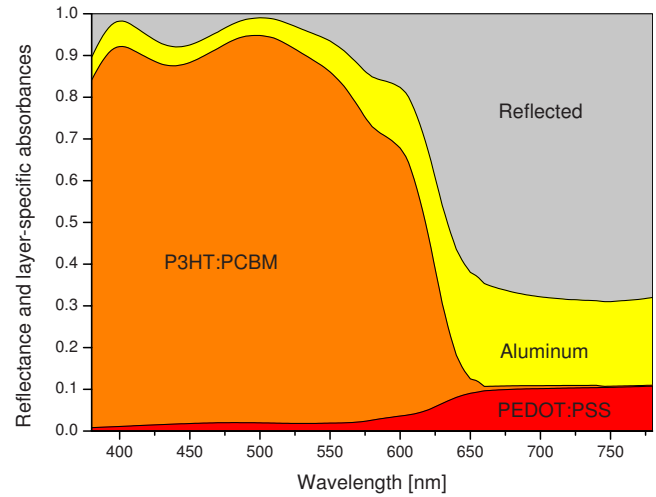


FIG. 2. (Color online) Reflectance and fractional absorbance for each layer in the solar cell.

field strength relative to the field strength in the surrounding medium E_0 . This is used to calculate the absolute energy flux by looking at the ratio

$$\frac{I}{I_0} = \frac{\frac{1}{2} \epsilon_0 c n |E|^2}{\frac{1}{2} \epsilon_0 c n_0 |E_0|^2} \quad (2)$$

of the illumination intensity I_0 in the surrounding medium and device internally I . In this study the AM 1.5 spectrum is used for I_0 . The calculation of the device internal intensity,

$$I = \frac{n}{n_0} |E_{\text{norm}}|^2 I_0, \quad (3)$$

is done wavelength and position dependent, from which the density of absorbed photons per second can be derived via

$$n_{\text{photons}} = \frac{\alpha I \lambda}{hc}, \quad (4)$$

where α stands for absorption coefficient which is given by $\alpha = 4\pi k / \lambda$ and k stands for the complex part of the refractive index (i.e., the extinction coefficient). After an integration over the illumination spectrum one ends up with a photon absorption rate profile [cf. Fig. 1 (bottom)]. The integration is done in the absorbing spectral range from 380 to 780 nm. The absorbance of the active layer, which is the ratio of absorbed to the illumination light intensity, drops to zero above 650 nm as is shown in Fig. 2. It is obvious that the thickness and refractive index are required for each layer for accurate simulation results. The n and k data were taken from Monestier *et al.*¹⁰

B. Electrical modeling

To simulate an OPV device electrically, several processes have to be taken into account. First charge-transfer-exciton generation and dissociation, then charge drift and diffusion, and at last the charge extraction at the electrodes need to be considered. These processes will be discussed in this section.

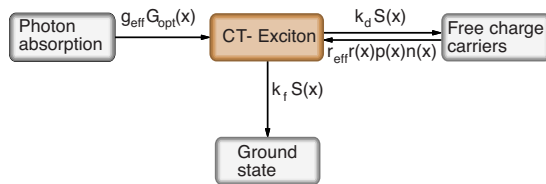


FIG. 3. (Color online) Relevant processes for CT-exciton modeling.

1. Charge-transfer-exciton dissociation

The absorption of a photon generates an exciton which then diffuses to a donor-acceptor interface. At this interface the exciton dissociates and generates a charge-transfer exciton (CT excitons). In this model we assume that a photon directly generates a CT exciton. Therefore, only a continuity equation for CT excitons is needed (cf. Fig. 3),

$$\frac{dS(x)}{dt} = r_{\text{eff}}r(x)p(x)n(x) - k_f S(x) - k_d S(x) + g_{\text{eff}}G_{\text{opt}}(x). \quad (5)$$

CT-exciton density S is fed by two processes: Firstly an absorbed photon directly generates a CT exciton. $G_{\text{opt}}(x)$ stands for the photon absorption profile shown in Fig. 1 (bottom), whereas g_{eff} is a photon-to-CT-exciton conversion efficiency. We set g_{eff} to zero outside of the active layer, which is P3HT:PCBM in the device under consideration here. Secondly recombination of free charge carrier pairs generates a CT exciton. This recombination process is treated by the Langevin theory which will be discussed in Sec. II B 2 when the drift-diffusion model is explained. There are also two CT-exciton state depletion mechanisms k_f and k_d which stand for the decay of a CT state and the dissociation, respectively, as described by the Onsager–Braun theory. This continuity equation for CT excitons is coupled with the drift-diffusion model which will be discussed later.

CT-exciton dissociation has been studied by Onsager.^{21,22} The initial pair separation distance is overestimated when measurements are compared with the Onsager theory. Therefore, Braun²³ extended the theory by Onsager. In this model a finite decay rate of the CT exciton has been considered. The dissociation probability P is then given by

$$P(T, E, k_f, a) = \frac{k_d}{k_d + k_f},$$

$$k_d(T, E, a) = \frac{3\mu e}{4\pi\epsilon a^3} e^{-[\Delta\mathcal{E}(a)/k_B T]} \frac{J_1[2\sqrt{-2b(T, E)}]}{-2b(T, E)},$$

$$\Delta\mathcal{E}(a) = \frac{e^2}{4\pi\epsilon\epsilon_0 a},$$

$$b(T, E) = \frac{e^3 E}{8\pi\epsilon\epsilon_0 k_B^2 T^2}. \quad (6)$$

In Eq. (6) the mobility is the sum of the electron and hole mobility $\mu = \mu_e + \mu_h$, $J_1(x)$ is the Bessel function of the first kind of order of 1, a is the initial pair separation distance of the CT exciton, and the pair binding energy $\Delta\mathcal{E}(a)$ is calculated under the assumption that CT excitons have the

same dependence of the binding energy on the separation distance as ion pairs. E stands for the electrical field which is calculated position dependent using the drift-diffusion model explained in Sec. II B 2.

To find an analytical model, the Onsager–Braun theory makes some simplifications. It does not consider disorder in energy levels as well as in the spatial distribution of the hopping sites which is present in an amorphous organic semiconductor. Koster *et al.*⁹ and Pan *et al.*²⁴ introduced spatial disorder by integrating the dissociation probability over distribution of pair separations a . A further simplification of the Onsager–Braun model is the assumption that the dissociation takes place in a homogeneous material, neglecting the presence of donors and acceptors. Veldman *et al.*²⁵ proposed that the mobility used in the Onsager–Braun model is higher than the effective mobility measured in the bulk. They attributed this to local crystallization of the PCBM molecules. This extension allows to model CT-exciton lifetimes in the order of 10^{-8} s still having a dissociation efficiency over 90%. This extension is not considered in our study. To analyze the effects of disorder and donor acceptor interfaces in more detail, Monte Carlo simulations are used which are not the scope of this study.^{26–33} Albeit all the simplifications, the Onsager–Braun theory is a widely used model to describe the dissociation of CT excitons in organic semiconductors.

2. Drift-diffusion modeling

In the semiconductor, the following drift-diffusion equations apply:

$$\frac{dE(x)}{dx} = \frac{e}{\epsilon_r \epsilon_0} [p(x) - n(x)], \quad (7)$$

$$J_e(x) = e\mu_e n(x)E(x) + D(\mu, T) \frac{dn(x)}{dx}, \quad (8)$$

$$\frac{dn(x)}{dt} = \frac{1}{e} \frac{dJ_e(x)}{dx} - r_{\text{eff}}r(x)p(x)n(x) + k_d S(x). \quad (9)$$

The electrical field $E(x)$ in Eq. (7) is calculated dependent on the position x . Where e stands for the elementary charge, $n(x)$, $p(x)$ for the electron/hole density, and ϵ_0 for the permittivity of free space and ϵ_r for the relative permittivity.

Equation (8) is the current equation for electrons. The mobility μ_e is shown to be independent of the electrical field, temperature, or density, which is a simplified assumption used in this paper. The diffusion coefficient is given by the Einstein relation: $D = \mu k_B T / q$.

Equation (9) is the continuity equation for electrons. This equation takes the creation, migration, and recombination of the charge carriers into account. $r(x)$ stands for the Langevin recombination $r(x) = (\mu_e + \mu_p)q / \epsilon_r \epsilon_0$. The requirement for this model to be applicable is that the mean free path $\lambda < r_c$, where r_c stands for the Coulombic capture radius $r_c = e^2 / 4\pi\epsilon_r \epsilon_0 k_B T$ which for an average organic solid ($\epsilon_0 \approx 3-4$) gives a Coulombic radius of $r_c \approx 14-19$ nm. This requirement is satisfied since the mean free path in this low-mobility disordered organic semiconductor is smaller than the Coulombic capture radius³⁴ and thus this model is appli-

cable. The Langevin recombination efficiency prefactor r_{eff} is a factor between 0 and 1 which has been introduced by Juška *et al.*³⁵ to take the reduced Langevin recombination into account. It will be discussed later in this paper.

For Eqs. (8) and (9) exist analogous equations for holes instead of electrons. The above set of equations is spatially discretized in SETFOS (Ref. 19) using the Scharfetter Gummel discretization³⁶ and solved iteratively in time using the Gummel scheme.³⁷

3. Built-in voltage

There is a debate on the nature of the open-circuit voltage V_{oc} in OPVs and currently there are several alternative explanations. There is evidence that the open-circuit voltage depends on the highest occupied molecular orbit (HOMO) and lowest occupied molecular orbit (LUMO) difference of the donor and acceptor molecules at the interface.^{38,39} Recently, this mechanism has been looked at in more detail and a linear dependence of the V_{oc} on the energy of the charge-transfer absorption has been found.⁴⁰ The open-circuit voltage also depends on the work function of the electrodes.⁴¹ This influence seems to be more pronounced in BHJ than in planar heterojunction device setups.⁴² Furthermore, the open-circuit voltage was observed to be intensity and temperature dependent.⁴³ This complex behavior is challenging for the simulation of these devices because there is not a single theory which is capable of describing all of those dependencies. The approach used here assumes that every device has a built-in voltage V_{bi} which is derived from the difference in the work functions of the two electrodes. This is then used to calculate the effectively applied voltage V_{eff} . The electric field distribution inside the device is obtained through integration of the Poisson equation [cf. Eq. (7)] using the effective bias V_{eff} as a constraint to determine the integration constant,

$$V_{\text{eff}} = V_{\text{appl}} - V_{\text{bi}} = \int E dx, \quad (10)$$

where V_{appl} is the experimentally applied voltage. Therefore, the electric field due to space charges is superimposed on the applied field.

4. Charge extraction

When charges reach the organic-metallic interface they are extracted from the device. The current at such an interface has been described by Scott *et al.*⁴⁴ as a balance of injection and surface recombination. This model considers the barrier reduction at an organic-metal interface due to the electric field and the image charge potential and calculates the net injection current.

5. Validation of the simulator

The model presented has been validated by varying the input parameters and analyzing their influence on the output. We have observed that the open-circuit voltage increases slightly with illumination intensity. It also depends on the mobility of the charge carriers. Furthermore, it is not equal to the built-in voltage which is assumed to be the difference

TABLE I. Input parameters for the thickness dependent simulation of Fig. 4.

Description	Parameter	Value Unit
Workfunction PEDOT		5 eV
Workfunction Al		4.31 eV
HOMO P3HT ^a		5.3 eV
LUMO PCBM ^a		3.7 eV
Electron mobility ^b	μ_n	$5 \times 10^{-7} \text{ m}^2/\text{V s}$
Hole mobility ^b	μ_p	$1 \times 10^{-8} \text{ m}^2/\text{V s}$

^aReference 46.

^bReference 45.

between the work functions of the electrodes in this model. The fill factor is influenced by recombination losses and thus the mobility of the charge carriers and the Langevin recombination efficiency r_{eff} . The short-circuit current depends linearly on the illumination intensity until recombination losses take over and the increase becomes sublinear. The results of this validation correspond to experimental observations.

III. ESTIMATION OF THE DISSOCIATION RATE

After describing the coupled optoelectronic numerical device model in Sec. II, it will be applied in this section to simulate an OPV device and extract unknown CT-exciton dissociation input parameters. The layer structure is shown in Fig. 1. The indium tin oxide (ITO) layer has a thickness of 130 nm, it is followed by a 50 nm thick poly(3,4-ethylenedioxythiophene):poly(styrenesulfonate) (PEDOT:PSS) layer. The active layer is modeled as a 1:1 weight ratio P3HT:PCBM blend which is covered by 100 nm aluminum. The parameters for the electrical simulations which are taken from literature are shown in Table I. The two mobilities are taken from Mihailetchi *et al.*,⁴⁵ who have measured the constant mobilities of electrons and holes in a P3HT:PCBM BHJ solar cell depending on the annealing temperature. The measurements used here are for samples which have been annealed at 140 °C for 5 min and the mobilities have been chosen accordingly.

The unknown parameters are the decay rate k_f , the pair separation distance a , and the photon-to-CT-exciton conversion efficiency g_{eff} which have been introduced in Eqs. (5) and (6), respectively. These parameters can be determined by applying the device model to thickness dependent measurements of the short-circuit current. Some reports in literature have used a simplified OPV model without CT-exciton dynamics (cf. Juška *et al.*³⁵) and have found reduced recombination rates. Similarly our first analysis step assumes that absorbed photons directly generate free electron hole pairs and that recombining charges are lost and not fed into the continuity equation for CT excitons (5). This reduced model thus consists of Eqs. (7) and (8) and the modified version of Eq. (9) which reads as follows:

$$\frac{dn(x)}{dt} = \frac{1}{e} \frac{dJ_e(x)}{dx} - r_{\text{eff}} r(x) p(x) n(x) + g_{\text{eff}} G_{\text{opt}}(x), \quad (11)$$

where g_{eff} stands for the photon-to-electron conversion efficiency.

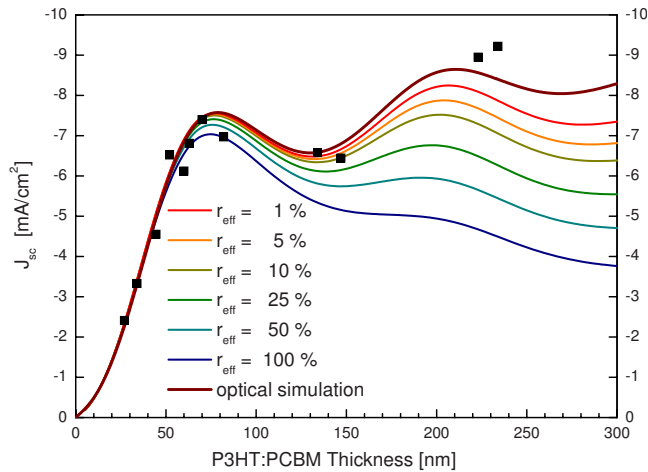


FIG. 4. (Color online) Thickness dependence of the short-circuit current J_{sc} with varying Langevin recombination efficiency r_{eff} . A purely optical simulation is also shown. The simulations are compared with measurements (■) by Gilot *et al.* (Ref. 20).

Figure 4 shows a purely optical simulation (top curve) to calculate the maximum achievable photocurrent depending on the device thickness. The other six curves are for coupled optoelectronic simulations where the Langevin recombination efficiency r_{eff} has been varied between 1 and 0.01. These simulation are compared with measurements by Gilot *et al.*²⁰ For devices with an active layer thickness below 50 nm electrical losses can be neglected. Therefore the photon-to-CT-exciton conversion efficiency g_{eff} is fitted to this part of the curve. A value of $g_{eff}=0.66$ has been determined which is consistent with the analysis by Gilot *et al.*²⁰ on the same thickness dependent data. For thicker devices electrical losses play an important role. Due to measurement uncertainties it is hard to give a final value, but Fig. 4 suggests that the Langevin recombination efficiency r_{eff} in the simplified model is 10% or lower. In the full model there is an equilibrium between CT-exciton formation and dissociation. We translate the observation of the reduced r_{eff} in the simple model to the dissociation probability in the full model, since the rate $r \times r_{eff}$ (simple model) corresponds to $r \times (1-P)$ (full model) [cf. with Eqs. (6) and (9)]. Thus P must be 90% or higher.

With this information it is possible to determine the unknown CT-exciton parameters by analyzing the Onsager-Braun model of CT-exciton dissociation. The initial pair separation distance a can be determined under the assumption that k_f is set to $1 \times 10^5 \text{ s}^{-1}$. The current density in Fig. 4 has been measured and calculated under short-circuit current conditions. From the open-circuit voltage which is about 0.6 V and the device thickness the internal electric field is estimated to be in the range of $1 \times 10^6 - 2 \times 10^7 \text{ V/m}$ for thick and thin devices, respectively. Figure 5 shows the desired dissociation efficiency (over 90%) and the internal electrical field range together with different initial pair separation distances which have been varied between 1.5 and 1 nm. From this plot alone the only condition for a is that it has to be larger than 1.2 nm. The best fit value for the pair separation distance a has been chosen to be 1.285 nm, by comparing experimental current-voltage curves with simulated

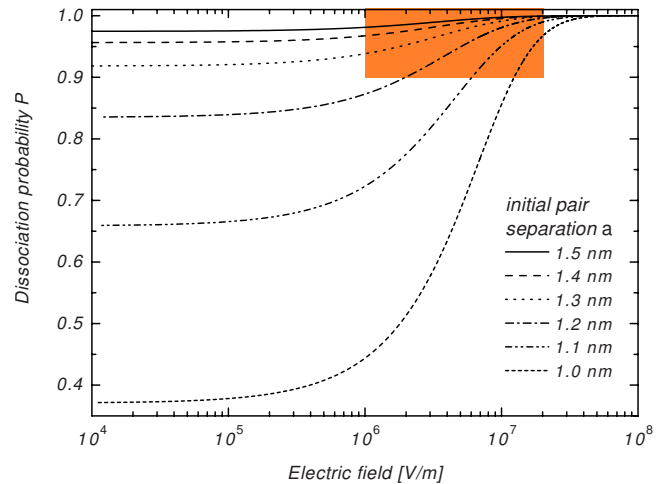


FIG. 5. (Color online) Dissociation probability according to the Onsager-Braun theory depending on the electrical field for several initial pair separation distances a . The decay rate has been kept fixed at $k_f=1 \times 10^5 \text{ s}^{-1}$.

curves for an active layer thickness of 70 nm (cf. Fig. 6). The thickness of 70 nm has been chosen because it is close to the first peak of the short-circuit current. Now, all the parameters for the full model are determined and summarized in Tables I and II. They are used in the following simulations where the full model including CT-exciton dissociation is considered.

Note that in the full model there is no need to reduce the recombination efficiency. Even though the original recombination rate is used (i.e., $r_{eff}=1$), there are small recombination losses due to the competing dissociation. Also note that the value of g_{eff} which was determined in the simple model is also applicable in the full model since with either model the parameter extraction is done by dividing the calculated theoretical maximum of the photocurrent by the measured one, preferably for thin devices where transport losses can be neglected.

IV. SENSITIVITY ANALYSIS

In Sec. III a set of parameters has been found (cf. Tables I and II) such that the simulation fits the measurements. In

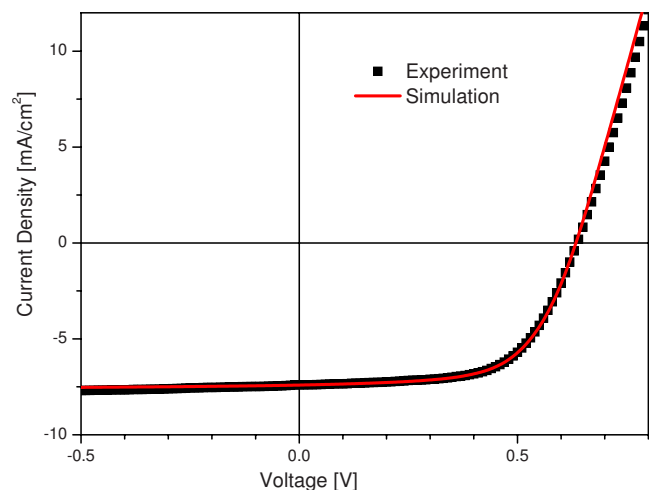


FIG. 6. (Color online) Comparison of a simulated and experimentally measured current-voltage curve for an active layer thickness of 70 nm. The parameters used for this simulation are summed up in Tables I and II.

TABLE II. Derived simulation parameters from Figs. 4–6.

Parameter	Symbol	Value Unit
Recombination eff.	r_{eff}	1
Decay rate	k_f	$1 \times 10^5 \text{ s}^{-1}$
Pair separation	a	1.285 nm
Optical generation eff.	g_{eff}	0.66

this section the sensitivity of the model on the input parameters is investigated. This sensitivity analysis gives insight into simulation as well as experiment: First we analyze and study which parameters influence the outcome of the simulation, secondly the sensitivity analysis also helps to identify experimental setups where the influence of different parameters can be separated.

The sensitivity analysis has been conducted as follows: Firstly, a reference has been simulated with the parameters indicated in Tables I and II. Secondly, five input parameters have been chosen, Langevin recombination efficiency r_{eff} , the electron/hole mobility μ_n/μ_p , the pair separation distance a , and the decay rate k_f . The first three parameters ($r_{\text{eff}}, \mu_n, \mu_p$) have been varied $\pm 10\%$, and because the influence of the CT-exciton parameters (a, k_f) is larger, these two parameters have been varied by 3% only. Therefore, in this step ten simulations have been done (five parameters with variation in two directions each). As a last step, the reference curve has then been subtracted from the varied curves. This difference between the reference curve and the varied one has then been plotted for each parameter. This procedure reveals possible orthogonalities among the parameters.

A. Thickness dependent sensitivity

First of all the thickness dependence of the short-circuit current has been analyzed, the results are shown in Fig. 7. The measurements are also shown and agree the simulation for active layer thicknesses up to 150 nm. The two measurements around 230 nm which are shown in Fig. 4 are lying outside the axis scale in Fig. 7 and cannot be modeled with the parameter set used in this study. This suggests that the different spin speed and solvent concentrations that have

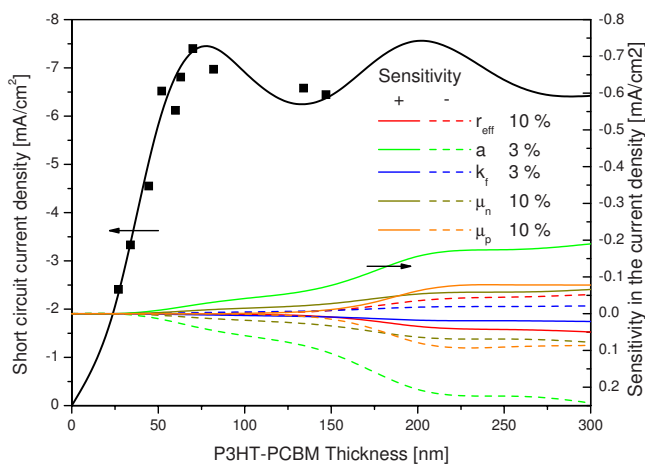


FIG. 7. (Color online) Sensitivity of the current density for a thickness dependent simulation.

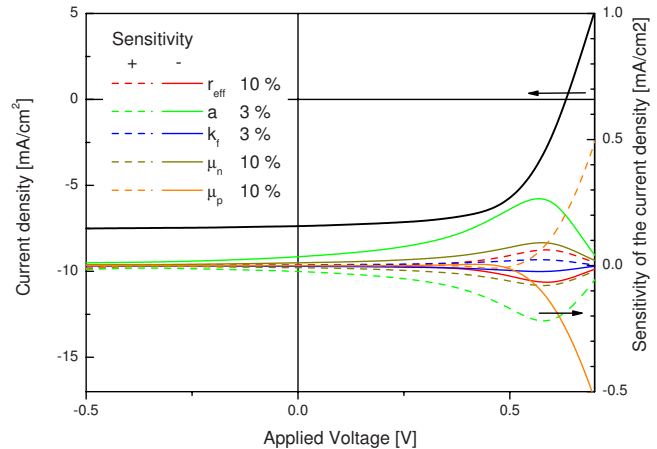


FIG. 8. (Color online) Sensitivity of the current density in for a current-voltage curve.

been used to achieve the higher active layer thicknesses²⁰ also changed electrical properties of the active layer and therefore cannot be modeled with a single set of parameters.

As is shown in Fig. 7, the influence of the electric input parameters is only relevant for an active layer thickness larger than about 50 nm, which has already been seen for the Langevin recombination efficiency in Fig. 4. The pair separation a has the highest influence on the short-circuit current although it has been varied by only 3%. The influence of all the parameters grows with increasing active layer thickness.

Further analysis, not shown here, reveals a strong linear dependence between the three parameter pair separation distance a , decay rate k_f and electron mobility μ_n . These three parameters are all involved in the dissociation of CT excitons [cf. Eq. (6)]. The thickness variation influences the electric field inside the device. Therefore, the electric field dependence of the CT-exciton dissociation is probed. The three parameters which show the same thickness dependence are all prefactors for the field dependence as shown in Eq. (6). In these equations the hole mobility is added to the electron mobility to determine the dissociation rate k_d , but in the device investigated here the electron mobility is higher by a factor of 50 than the hole mobility and therefore dominates the dissociation. The hole mobility μ_p and the Langevin recombination efficiency r_{eff} both have a unique thickness dependence, which is slightly different from each other.

B. Current-voltage curve sensitivity

Figure 8 shows the sensitivity analysis for a current-voltage curve with an active layer thickness of 70 nm. The current-voltage curve is the same one as in Fig. 6. The sensitivity analysis clearly demonstrates that all parameters have the highest influence on the current-voltage curve in the fourth quadrant and close to the open-circuit voltage V_{oc} . Again the pair separation distance a has the strongest influence on the output. The hole mobility clearly has a different influence on the output than all the other parameters. Especially for applied voltages which are higher than V_{oc} the hole mobility has the highest influence on the current. This suggests that the hole mobility is the limiting factor for the current (photocurrent plus injected current) drawn from the

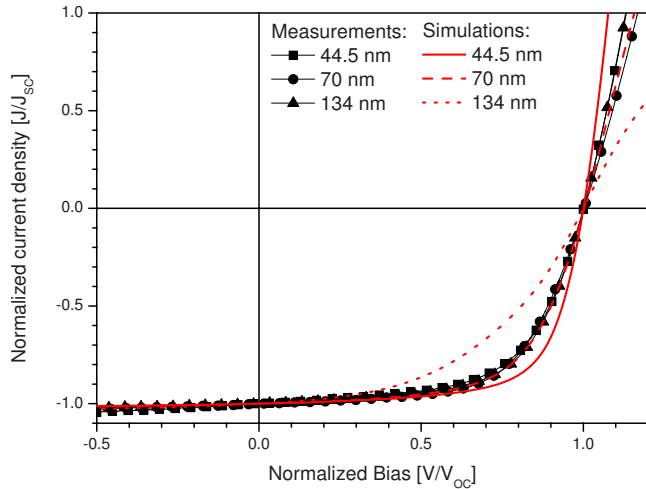


FIG. 9. (Color online) Normalized comparison between measured and simulated J - V curves for different active layer thicknesses.

device at higher voltages. Further analysis (not shown) reveals that for the current-voltage curve under consideration there are only two clearly linearly independent sets of parameters. The first set comprises the pair separation a , the decay rate k_f , the electron mobility μ_n , and the Langevin recombination efficiency r_{eff} , the second one is the hole mobility μ_p . Although the Langevin recombination has a slightly different voltage behavior than the other three parameters in this group it is very similar. This is interesting because in the sensitivity analysis of the thickness dependent short-circuit current shown in Fig. 7 the influence of the Langevin recombination efficiency was more similar to the one of the hole mobility.

For all the measured short-circuit current points in Fig. 4 a current-voltage curve was measured as well. An analysis of the influence of the device thickness on the current-voltage curve is performed for three representative thicknesses which is shown in Fig. 9. The short-circuit current as well as the open-circuit voltage depends on the amount of the absorbed photons. Therefore, to compare the current-voltage curves for different thicknesses the short-circuit current as well as the open-circuit voltage needs to be normalized to exclude optical effects. The comparison in Fig. 9 shows that the shape of the experimental current-voltage curve does not change for different thicknesses of the active layers. In contrast the simulated current-voltage curves show a clear dependence of the shape on the device thickness. This indicates that in the fourth quadrant the influence of the electric field on dissociation efficiency and thus recombination losses is overestimated in the device model presented here. A possible explanation for this discrepancy might be the nature of the Onsager–Braun dissociation mechanism, which does not consider energetic disorder. Although much used, the Onsager–Braun model is not necessarily the best physical description of charge separation and more refined models have been developed. For instance Wojcik *et al.*⁴⁷ have derived an extended model based on the Onsager theory which leads to a weaker field dependence.

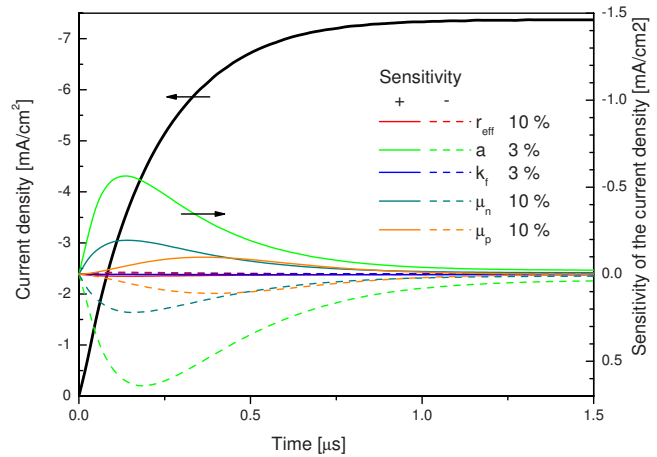


FIG. 10. (Color online) Sensitivity of the short-circuit current during turn-on.

C. Transient current sensitivity

The sensitivity analyses in thickness dependence and current-voltage curves have shown that several input parameters have a similar influence on the output and thus those parameters cannot be determined from these measurements. In this part transient simulations are discussed and their sensitivity on parameters is analyzed.

Figure 10 shows the simulated transient of the short-circuit current when the light is turned on at $t=0$ for a thickness of the active layer of 70 nm. Again the parameter set shown in Table I and II has been used. The sensitivity clearly shows that in the turn-on dynamics the Langevin recombination efficiency r_{eff} and the decay rate k_f do not play an important role, therefore the turn-on dynamics is solely defined by the pair separation distance a and the two mobilities. The CT-exciton decay rate and thus the recombination of free charge carriers play no role. The electron mobility determines the first part of the turn-on and the sensitivity reaches its maximum at $0.15 \mu\text{s}$, whereas the hole mobility has its maximum at $0.35 \mu\text{s}$. Further analysis (not shown) reveals that the electron mobility μ_n has exactly the same influence on the turn-on behavior as does the pair separation a . This indicates that the turn-on behavior is limited by the time it takes to dissociate the CT-exciton pair. When the CT-exciton parameters are chosen such that the average lifetime of the CT exciton is much smaller than the time it takes to extract the charge carriers, the turn-on behavior is solely defined by the two mobilities.

Figure 11 shows the transient of the short-circuit current when the light is turned off at $t=0$. The shape of the transient turn-off curve shown in Fig. 11 is clearly different from the turn-on curve shown in Fig. 10. The first one has a clearly visible kink at $t=0.015 \mu\text{s}$, whereas the latter curve is more smooth without any visible kink. The sensitivity analysis of the turn-off behavior shows that the curve is solely dependent on the two mobilities. This means that CT exciton and recombination parameters play no role and thus the recombination and subsequent CT-exciton dissociation play no role. The initial drop is given by the mobility of the electrons μ_n whose influence peaks at $t=0.01 \mu\text{s}$, whereas the second, much slower drop is given by the hole mobility μ_p whose

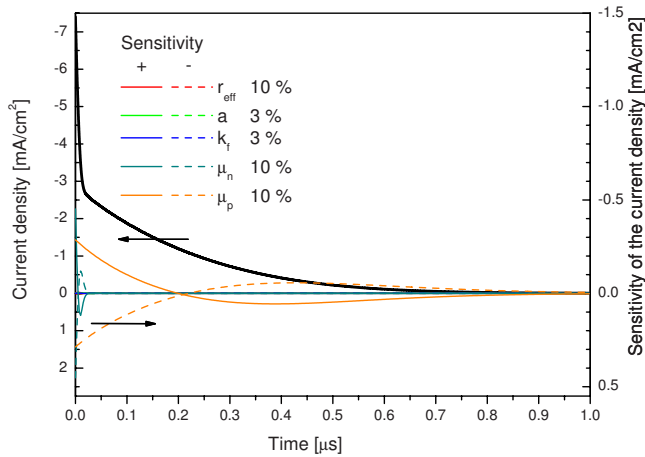


FIG. 11. (Color online) Sensitivity of the short-circuit current during turn-off.

influence peaks at $t=0.45 \mu\text{s}$. This difference is in the same range as the difference in the mobilities of the two charge carriers which is $\mu_n/\mu_p=50$.

This last sensitivity analysis shows that by measuring the short-circuit current during turn-off, the two mobility parameters can be estimated. This observation is similar to the findings by Pinner *et al.*⁴⁸ for electroluminescence transients in organic light-emitting diodes where the turn-off regime is governed by the built-in field as well. The time it takes to extract all charge carriers and thus the mobilities can be calculated under the assumption that the active layer is homogeneously filled with charge carriers and that the internal electric field is given by the difference on the applied and the built-in voltage divided by the active layer thickness $E=(V-V_{bi})/L$. We thus obtain

$$\mu = \frac{L^2}{(V_{\text{appl}} - V_{\text{bi}})\tau}. \quad (12)$$

The parameter τ is the time it takes for the current to drop down to 5% of the initial value. With this approach the electron as well as the hole mobility can be extracted separately.

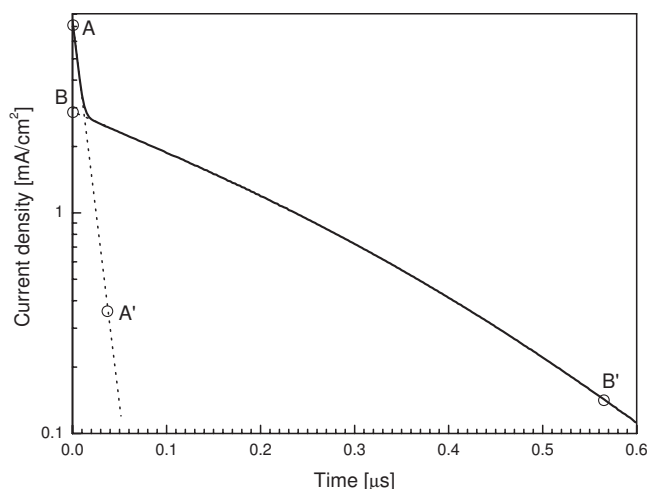


FIG. 12. Semilogarithmic plot of the turn-off behavior shown in Fig. 11. This plot can be used to extract the mobilities of electrons and holes.

Figure 12 shows the turn-off behavior as a semilogarithmic plot. The first steep drop of the current is associated with the electrons and thus a line is fitted to it. Point A' is defined as the point along the fitted curve where the initial current at point A is reduced to 5%. The same is done for the second drop which is associated with the holes. Again B' is defined as the point where the current dropped down to 5% with B as the reference point. This gives for $\tau_n=0.037 \mu\text{s}$ and $\tau_p=0.56 \mu\text{s}$. With $V_{\text{appl}}-V_{\text{bi}}=0.69 \text{ V}$ (cf. Table I) and an active layer thickness of 70 nm the following mobilities are extracted: $\mu_n=1.9 \times 10^{-7} \text{ m}^2/\text{V s}$ and $\mu_p=1.3 \times 10^{-8} \text{ m}^2/\text{V s}$. The extracted values are in the same order of magnitude as the input values given in Table I. The mobility of the fast charge carriers is underestimated and the mobility of the slow charge carriers is slightly overestimated. This discrepancies stem from the assumption of a homogeneous electric field inside the device and thus the independent treatment of electrons and holes which is a simplification.

V. CONCLUSION

From the measured thickness dependent short-circuit current for thin active layers and the optical model we estimated a photon to CT-exciton conversion efficiency g_{eff} of 66%. Using this dataset the coupled optoelectronic simulation suggests a lower limit for the CT-exciton dissociation efficiency of 90%. Adding the measured current-voltage curve to the numerical analysis and assuming that k_f is equal to $1 \times 10^5 \text{ s}^{-1}$, we find dissociation parameters that are consistent with the estimated 90% dissociation efficiency. From a comparison of several current-voltage curves at different thicknesses there is evidence that the influence of the electric field on the CT-exciton dissociation process is overestimated using the Onsager-Braun model. Further investigations have to be carried out to clarify this issue. The sensitivity analysis conducted demonstrates that the influence of the two exciton parameters and the electron mobility are linearly dependent in the current-voltage curve and photocurrent thickness scaling. A sensitivity analysis of transient processes indicates that the input parameters can be separated. During turn-on, the CT-exciton decay rate k_f and thus the charge carrier recombination play no role. Even more insight can be gained by looking at the turn-off behavior. In this regime the transient current density is solely defined by the mobilities of the charge carriers. This suggests that the charge carrier mobilities can be extracted. The influence of charge traps was not considered in this study but will be discussed elsewhere.

ACKNOWLEDGMENTS

We would like to thank Jan Gilot and Professor René A. J. Janssen from TU Eindhoven for supplying us with a consistent set of measurements and helpful discussions. The authors gratefully acknowledge financial support of the Swiss Federal Office of Energy.

¹M. A. Green, K. Emery, Y. Hishikawa, and W. Warta, *Prog. Photovoltaics* **17**, 320 (2009).

²J. Y. Kim, K. Lee, N. E. Coates, D. Moses, T.-Q. Nguyen, M. Dante, and A. J. Heeger, *Science* **317**, 222 (2007).

³J. Kalowekamo and E. Baker, *Sol. Energy* **83**, 1224 (2009).

- ⁴M. Harrison, J. Gruner, and G. Spencer, *Phys. Rev. B* **55**, 7831 (1997).
- ⁵L. A. A. Pettersson, L. Roman, and O. Inganäs, *J. Appl. Phys.* **86**, 487 (1999).
- ⁶F. Monestier J.- J. Simon, P. Torchio, L. Escoubas, B. Ratier, W. Hojeij, B. Lucas, A. Moliton, M. Cathelinaud, C. Defranoux, and F. Flory, *Appl. Opt.* **47**, C251 (2008).
- ⁷G. Dennler, K. Forberich, T. Ameri, C. Waldauf, P. Denk, C. J. Brabec, K. Hingerl, and A. J. Heeger, *J. Appl. Phys.* **102**, 123109 (2007).
- ⁸J. A. Barker, C. M. Ramsdale, and N. C. Greenham, *Phys. Rev. B* **67**, 075205 (2003).
- ⁹L. J. A. Koster, E. C. P. Smits, V. D. Mihailetchi, and P. W. M. Blom, *Phys. Rev. B* **72**, 085205 (2005).
- ¹⁰F. Monestier, J. Simon, P. Torchio, L. Escoubas, F. Flory, S. Bailly, R. Debettignies, S. Guillerez, and C. Defranoux, *Sol. Energy Mater. Sol. Cells* **91**, 405 (2007).
- ¹¹C. Deibel, A. Wagenpfahl, and V. Dyakonov, *Phys. Status Solidi (RRL)* **2**, 175 (2008).
- ¹²I. Hwang and N. C. Greenham, *Nanotechnology* **19**, 424012 (2008).
- ¹³T. Kirchartz, B. E. Pieters, K. Taretto, and U. Rau, *J. Appl. Phys.* **104**, 094513 (2008).
- ¹⁴S. Lacic and O. Inganäs, *J. Appl. Phys.* **97**, 124901 (2005).
- ¹⁵J. D. Kotlarski, P. W. M. Blom, L. J. A. Koster, M. Lenes, and L. H. Slooff, *J. Appl. Phys.* **103**, 084502 (2008).
- ¹⁶J. Leger, S. Carter, B. Ruhstaller, H. Nothofer, U. Scherf, H. Tillman, and H. Horhold, *Phys. Rev. B* **68**, 054209 (2003).
- ¹⁷B. Ruhstaller, S. Carter, S. Barth, H. Riel, W. Riess, and J. Scott, *J. Appl. Phys.* **89**, 4575 (2001).
- ¹⁸B. Ruhstaller, T. Beierlein, H. Riel, S. Karg, J. Scott, and W. Riess, *IEEE J. Sel. Top. Quantum Electron.* **9**, 723 (2003).
- ¹⁹Semiconducting thin film optics simulator (SETFOS) by Fluxim AG, Switzerland (www.fluxim.com).
- ²⁰J. Gilot, I. Barbu, M. M. Wienk, and R. A. J. Janssen, *Appl. Phys. Lett.* **91**, 113520 (2007).
- ²¹L. Onsager, *J. Chem. Phys.* **2**, 599 (1934).
- ²²L. Onsager, *Phys. Rev.* **54**, 554 (1938).
- ²³C. L. Braun, *J. Chem. Phys.* **80**, 4157 (1984).
- ²⁴J. Pan and D. Haarer, *Chem. Phys. Lett.* **324**, 411 (2000).
- ²⁵D. Veldman, O. Ipek, S. C. J. Meskers, J. Sweelssen, M. M. Koetse, S. C. Veenstra, J. M. Kroon, S. S. van Bavel, J. Loos, and R. A. J. Janssen, *J. Am. Chem. Soc.* **130**, 7721 (2008).
- ²⁶F. Stolzenburg, B. Ries, and H. Bassler, *Ber. Bunsenges. Phys. Chem.* **91**, 853 (1987).
- ²⁷U. Albrecht and H. Bassler, *Chem. Phys. Lett.* **235**, 389 (1995).
- ²⁸V. Arkhipov, H. Bässler, E. Emelyanova, D. Hertel, V. Gulbinas, and L. Rothberg, *Macromol. Symp.* **212**, 13 (2004).
- ²⁹T. Offermans, S. Meskers, and R. A. J. Janssen, *Chem. Phys.* **308**, 125 (2005).
- ³⁰C. Groves, R. A. Marsh, and N. C. Greenham, *J. Chem. Phys.* **129**, 114903 (2008).
- ³¹R. A. Marsh, C. Groves, and N. C. Greenham, *J. Appl. Phys.* **101**, 083509 (2007).
- ³²F. Yang and S. R. Forrest, *ACS Nano* **2**, 1022 (2008).
- ³³E. V. Emelianova, M. V. D. Auweraer, and H. Bässler, *J. Chem. Phys.* **128**, 224709 (2008).
- ³⁴M. Pope and C. E. Swenberg, *Electronic Processes in Organic Crystals and Polymers* (Oxford University Press, New York, 1999).
- ³⁵G. Juska, K. Arlauskas, J. Stuchlik, and R. Osterbacka, *J. Non-Cryst. Solids* **352**, 1167 (2006).
- ³⁶D. Scharfetter and H. Gummel, *IEEE Trans. Electron Devices* **16**, 64 (1969).
- ³⁷H. Gummel, *IEEE Trans. Electron Devices* **11**, 455 (1964).
- ³⁸C. Brabec, A. Cravino, D. Meissner, N. Sariciftci, T. Fromherz, M. Rispiens, L. Sanchez, and J. Hummelen, *Adv. Funct. Mater.* **11**, 374 (2001).
- ³⁹C. Brabec, A. Cravino, D. Meissner, N. Sariciftci, M. Rispiens, L. Sanchez, J. Hummelen, and T. Fromherz, *Thin Solid Films* **403**, 368 (2002).
- ⁴⁰K. Vandewal, A. Gadisa, W. D. Oosterbaan, S. Bertho, F. Banishoeib, I. V. Severen, L. Lutsen, T. J. Cleij, D. Vanderzande, and J. V. Manca, *Adv. Funct. Mater.* **18**, 2064 (2008).
- ⁴¹K. Kawano, N. Ito, T. Nishimori, and J. Sakai, *Appl. Phys. Lett.* **88**, 073514 (2006).
- ⁴²C. Uhrich, D. Wynands, S. Olthof, M. K. Riede, K. Leo, S. Sonntag, B. Maennig, and M. Pfeiffer, *J. Appl. Phys.* **104**, 043107 (2008).
- ⁴³L. J. A. Koster, V. D. Mihailetchi, R. Ramaker, and P. W. M. Blom, *Appl. Phys. Lett.* **86**, 123509 (2005).
- ⁴⁴J. Scott and G. Malliaras, *Chem. Phys. Lett.* **299**, 115 (1999).
- ⁴⁵V. Mihailetchi, H. Xie, B. De Boer, L. Koster, and P. Blom, *Adv. Funct. Mater.* **16**, 699 (2006).
- ⁴⁶J. Kim, S. Kim, H.-H. Lee, K. Lee, W. Ma, X. Gong, and A. Heeger, *Adv. Mater. (Weinheim, Ger.)* **18**, 572 (2006).
- ⁴⁷M. Wojcik and M. Tachiya, *J. Chem. Phys.* **130**, 104107 (2009).
- ⁴⁸D. Pinner, R. Friend, and N. Tessler, *J. Appl. Phys.* **86**, 5116 (1999).